Supplemental Tables

Table S1. The list of primers and Taqman probes used in PCR and genotyping.

Name	Sequence	Experiment
ccdc39-F primer	CAGTGGGAGAACACCATTGAG	qRT-PCR and Sanger sequencing
ccdc39-R primer	TCTTGCTTCCTGCTTTATTCGTG	qRT-PCR and Sanger sequencing
b-actin-F primer	GGCTGTATTCCCCTCCATCG	qRT-PCR and Sanger sequencing
b-actin-R primer	CCAGTTGGTAACAATGCCATGT	qRT-PCR and Sanger sequencing
ccdc39-Ex10R primer	CTATGCCCAATTGAACCTCC	Sanger sequencing
ccdc39-Ex8R primer	CCTCAGAGCTTGTAAGTCAC	Sanger sequencing
prh-ccdc39 F primer	GTCACGAAGGCAACAGAAGTC	TaqMan SNP Genotyping assay
prh-ccdc39 R primer	GCCACTGAGCTTCTGTGTGA	TaqMan SNP Genotyping assay
prh-ccdc39 wt probe	AAGGATGAGGTGTGTCAC	TaqMan SNP Genotyping assay
prh-ccdc39 prh mutant probe	AGGATGAGGAGTGTCAC	TaqMan SNP Genotyping assay

Table S2. The list of antibodies used in immunofluorescence and western blotting

Name	Host	Dilution	Manufactured	ID	Usage
Acetylated α-tubulin	Mouse	1:1,000	Sigma	T7451	IHC with antigen retrieval
Arl13B	Rabbit	1:500	Proteintech	1711-1-AP	IHC with antigen retrieval
beta-tubulin	Mouse	1:1,000	Sigma	T8660	Western blotting
Ccdc39	Rabbit	1:1,000	Sigma	HPA035364 (A60704)	IHC, Western blotting
Dnali1	Rabbit	1:200	Proteintech	17601-1-AP	IHC
gamma-tubulin	Mouse	1:500	Sigma	T6557	IHC
Gas8	Rabbit	1:200	Gift from Dr. Mary Porter, University of Minnesota		IHC
GFAP	Rabbit	1:1,000	Sigma	G9296	Western blotting
MBP	Rabbit	1:1,000	Sigma	ab40390	Western blotting
anti-rabbit IgG-Alexa 488	Donkey	1:1,000	Thermo Fisher Scientific	A-21206	IHC
anti-rabbit IgG-Alexa 568	Donkey	1:1,000	Thermo Fisher Scientific	A10042	IHC
anti-mouse IgG-Alexa 488	Donkey	1:1,000	Thermo Fisher Scientific	A-21202	IHC
anti-mouse IgG-Alexa 568	Donkey	1:1,000	Thermo Fisher Scientific	A10037	IHC
IRDye® 680RD anti-Rabbit IgG	Goat	1:10,000	Licor	925-68071	Western blotting
IRDye® 680RD anti-Mouse IgG	Goat	1:10,000	Licor	925-68071	Western blotting

Supplemental Movies

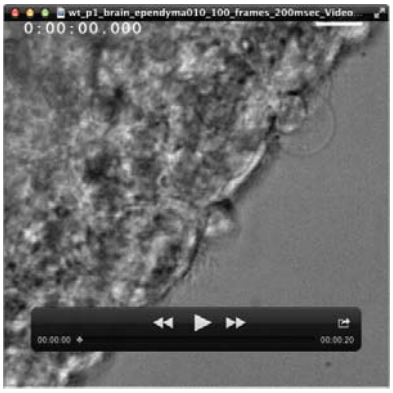

Movie 1: *Ex-vivo* video-microscopy recording of the P1 wild-type forebrain medial wall ependymal cilia.
P1 ependymal cilia in the *Ccdc39*$^{wt/wt}$ medial wall of the forebrain are motile and display normal beating pattern (video captured at a rate of 400 frames per second and played back at a rate of 5 frames per second), scale bar is 10 µm.

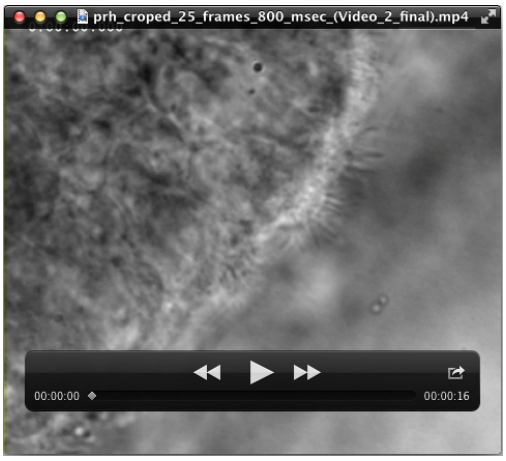

Movie 2: *Ex-vivo* video-microscopy recording of the P1 *Ccdc39*$^{prh/prh}$ forebrain medial wall ependymal cilia.

P1 *Ccdc39*$^{prh/prh}$ ependymal cilia of the medial forebrain wall are immotile and show rigid cilia beating patterns (video captured at a rate of 100 frames per second and played back at a rate of 5 frames per second), scale bar is 10 µm.

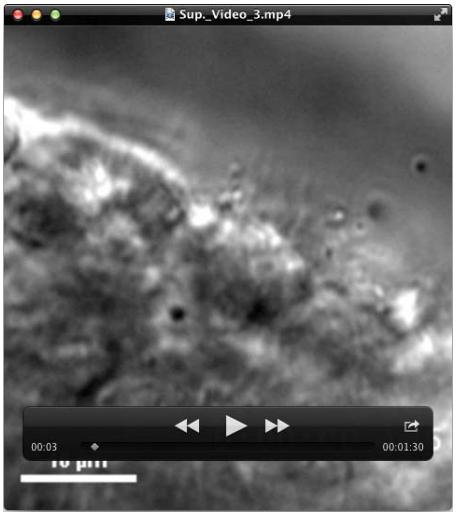

Movie 3: *Ex-vivo* video-microscopy recording of the wild-type forebrain medial wall ependymal cilia.

P6 ependymal motile cilia in medial wall of the forebrain displaying normal beating pattern, frequency, and cilia beating patterns (video captured at a rate of 100 frames per second and played back at 5 frames per second). Scale bar is 10 µm.

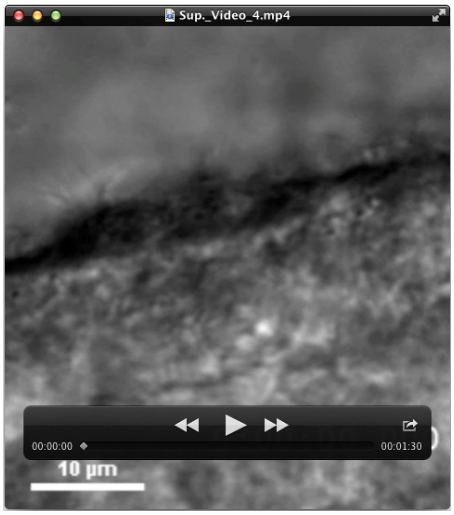

Movie 4: *Ex-vivo* video-microscopy recording of the *Ccdc39*$^{prh/prh}$ forebrain medial wall ependymal cilia.

P6 *Ccdc39*$^{prh/prh}$ ependymal motile cilia in medial wall of the forebrain showing slower beat frequency and a rigid cilia beating patterns (video captured at a rate of 100 frames per second and played back at 5 frames per second) than the wild-type cilia. Scale bar is 10 µm.

Movie 5: *Ex-vivo* video-microscopy recording of ependymal cilia-generated CSF flow in the central aqueduct of a wild-type mouse.

P7 ependymal motile cilia in the central aqueduct generating vigorous unidirectional CSF fluid flow (video captured at a rate of 10.4 frames per second and played back at 5 frames per second) in wild-type mouse. Scale bar is 10 µm.

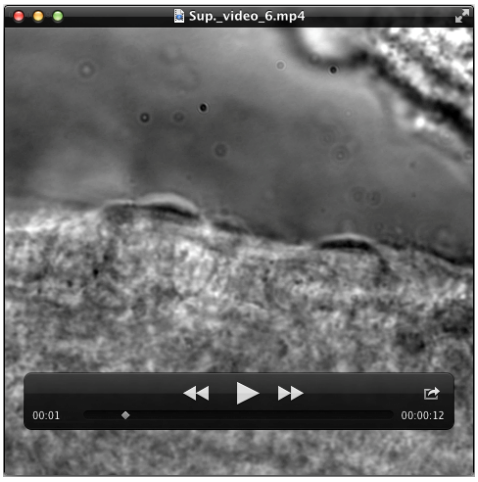

Movie 6: *Ex-vivo* video-microscopy recording of ependymal cilia-generated CSF flow in the central aqueduct of a *Ccdc39*$^{prh/prh}$ mouse.

The P7 ependymal cilia of the *Ccdc39*$^{prh/prh}$ central aqueduct showing rigid axoneme and are unable to generate CSF fluid flow (video captured at a rate of 10.4 frames per second and played back at 5 frames per second). Scale bar is 10 µm.

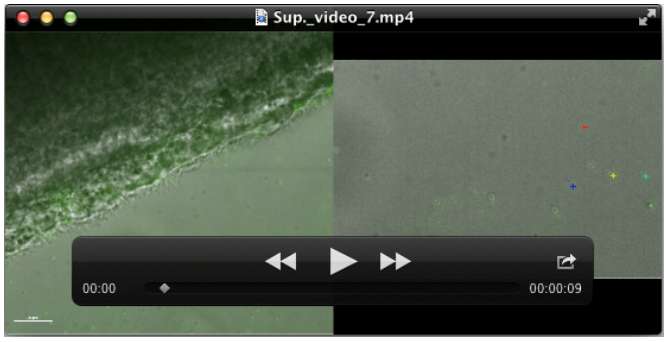

Movie 7: *Ex-vivo* video-microscopy tracing of fluorescent micro-beads in the wild-type mouse forebrain.
The original video of an *ex-vivo* brain slice with addition of fluorescent micro-beads in the P7 *Ccdc39*$^{wt/wt}$ forebrain ventricle (left). The enlarged and cropped video analyzed in NIS Element software (right). Tracking of the fluorescent micro-beads in the wild-type brain showed that the beads flowed quickly in one direction and exit the field of view very rapidly (video captured at rate of 41 frames per second were played back at a rate of 5 frames per second). Average flow speed was 68 ±0.7 µm/sec. Scale bar is 20 µm.

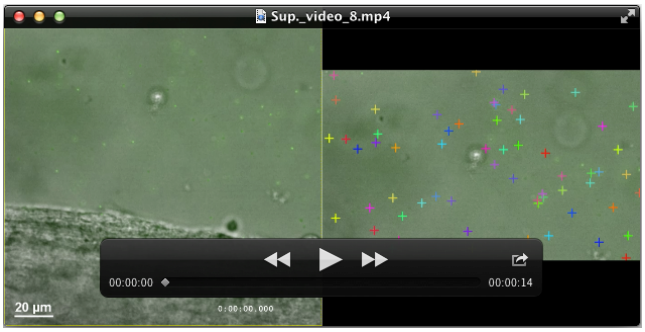

Movie 8: *Ex-vivo* video-microscopy tracing of fluorescent micro-beads in the *Ccdc39*$^{prh/prh}$ mutant forebrain.
The original video of an *ex-vivo* brain slice with addition of fluorescent micro-beads in the P7 *Ccdc39*$^{prh/prh}$ forebrain ventricle (left). The enlarged and cropped video analyzed in NIS Element software (right). Tracking of the fluorescent micro-beads in the *Ccdc39*$^{prh/prh}$ animals, the beads flowed very slowly in a multiple directions and can be detected in the field of view during the video recording (video captured at rate of 41 frames per second and were played back at a rate of 5 frames per second). Average flow speed was 11 ± 0.07 µm/sec. Scale bar is 20 µm.

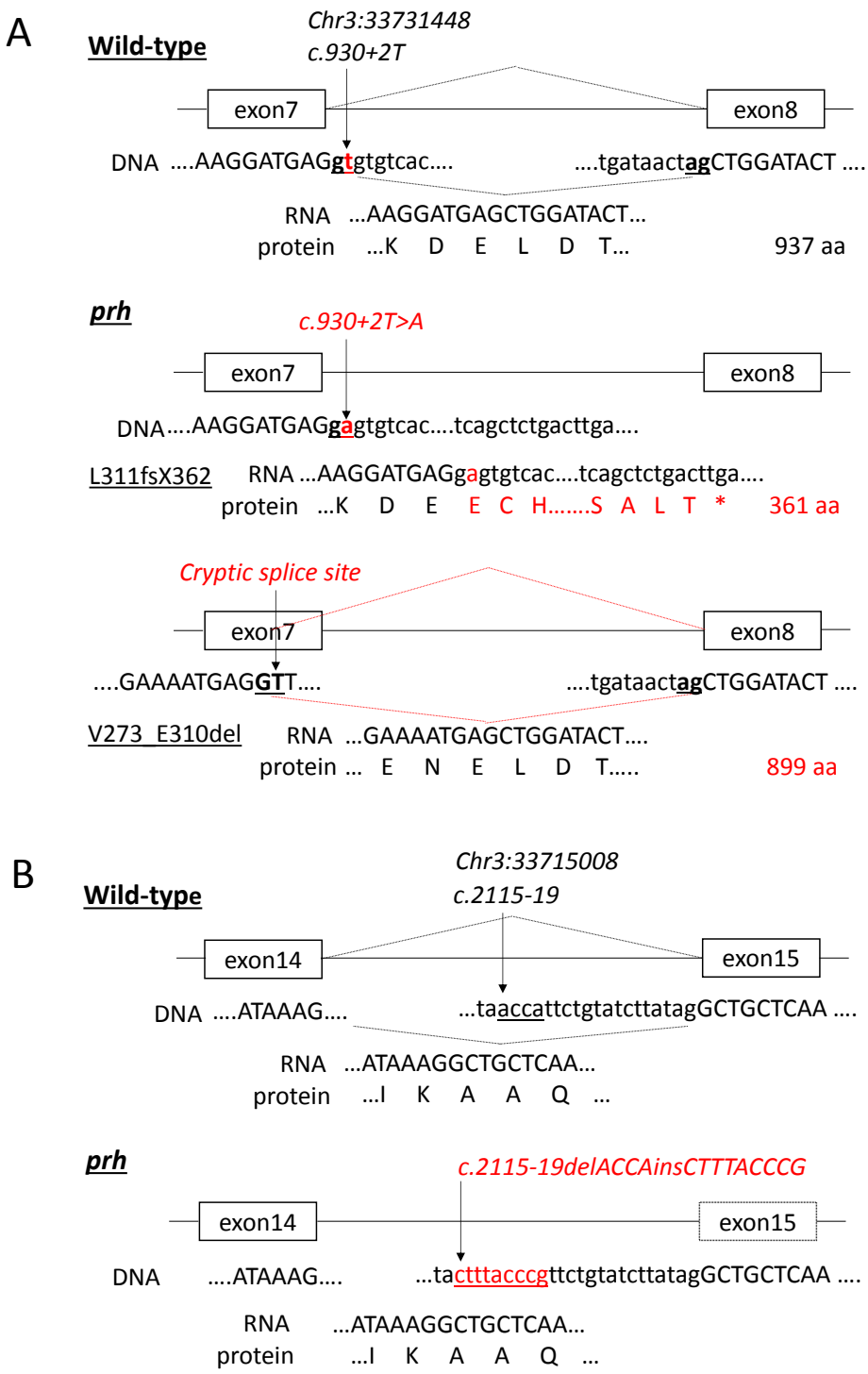

Supplemental Figure 1. Homozygous nucleotide sequence alterations found in the *prh* mutant.

(A) *Ccdc39*$^{c.930+2T>A}$ (g.chr3:33731488A>T) resulted in expression of two mRNA variants which encode Ccdc39L311fsX362, due to failure in mRNA splicing between exon 7 and exon 8, and Ccdc39V273_E310del due to cryptic splicing in the middle of exon 7, respectively. Neither of mutant proteins were stable and were not detected in western blotting.

(B) *Ccdc39*$^{c.2115-19delACCAinsCTTTACCCG}$ (g.33715005_8delinsCGGGTAAAG) did not affect the splicing between exon 14 and exon 15.

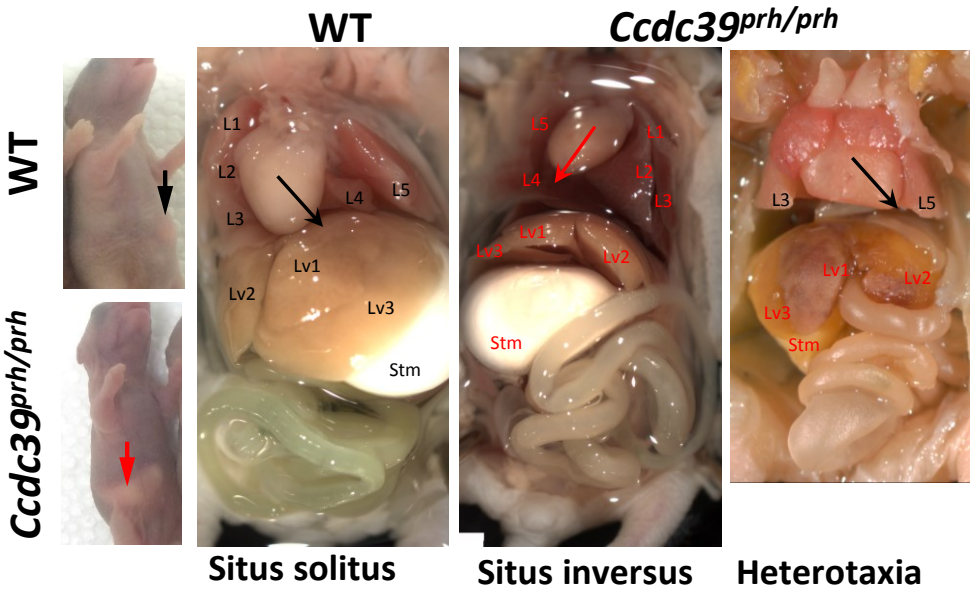

Supplemental Figure 2. The randomization of the left-right body asymmetry in the *Ccdc39*$^{prh/prh}$ mutant mice.

The right-sided stomach (identified by the milk spot) (5/15), situs inversus (3/15), and heterotaxia (2/15) were found in 15 mutants tested at P4. Dextrocardia was found in the mutants with situs inversus phenotypes (3/3).

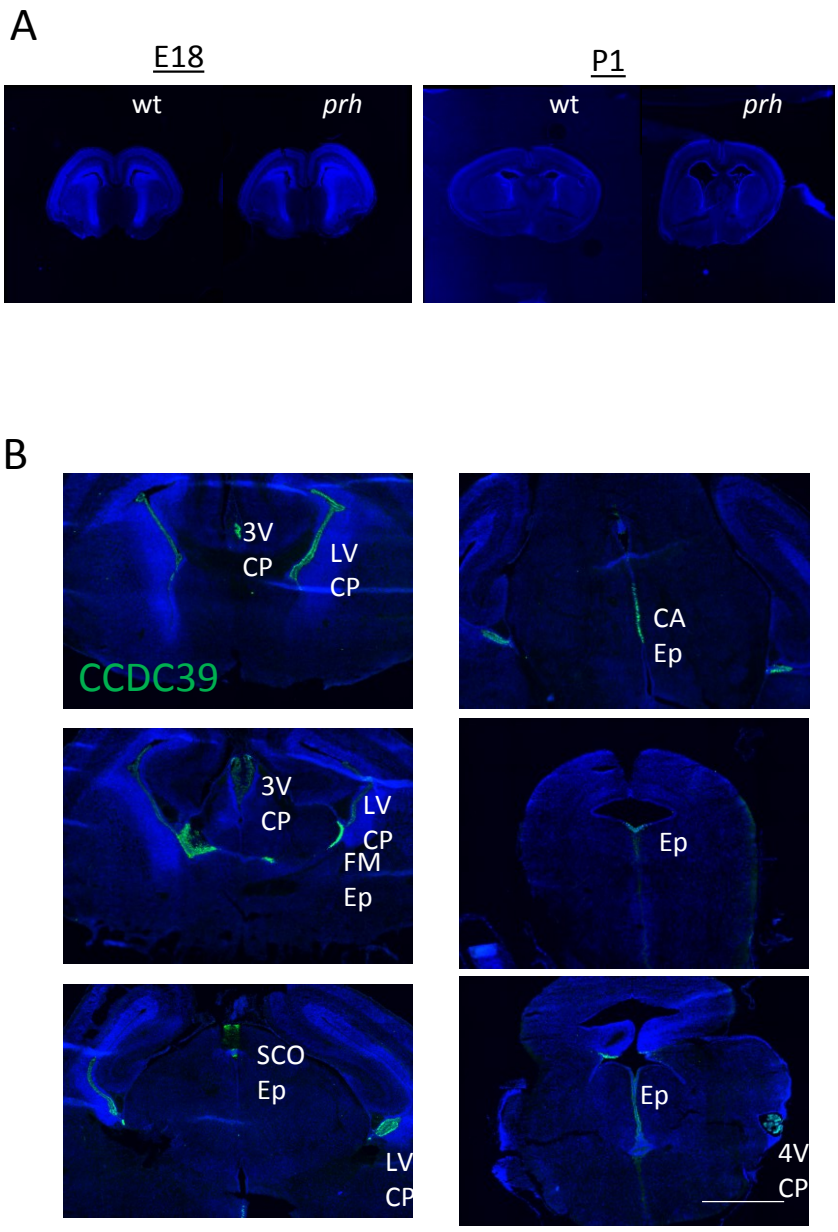

Supplemental Figure 3. Immunohistochemistry using CCDC39 antibody and brain histology of the *prh* mutant.
(A) Coronal brain sections of E18 and P1 *prh* mice and littermate controls. Ventriculomegaly was seen in P1 *prh* mice but not in E18.
(B) Immunohistochemistry using CCDC39 antibody expression in E18 mouse brain. CCDC39 is expressed in choroid plexus (CP) in lateral (LV), third (3V), and fourth (4V) ventricles, subcommissural organ (SCO), and ependymal (Ep) cells in ventromedial walls of the foramen of Monroe, and the central aqueduct. Scale bar, 1 mm

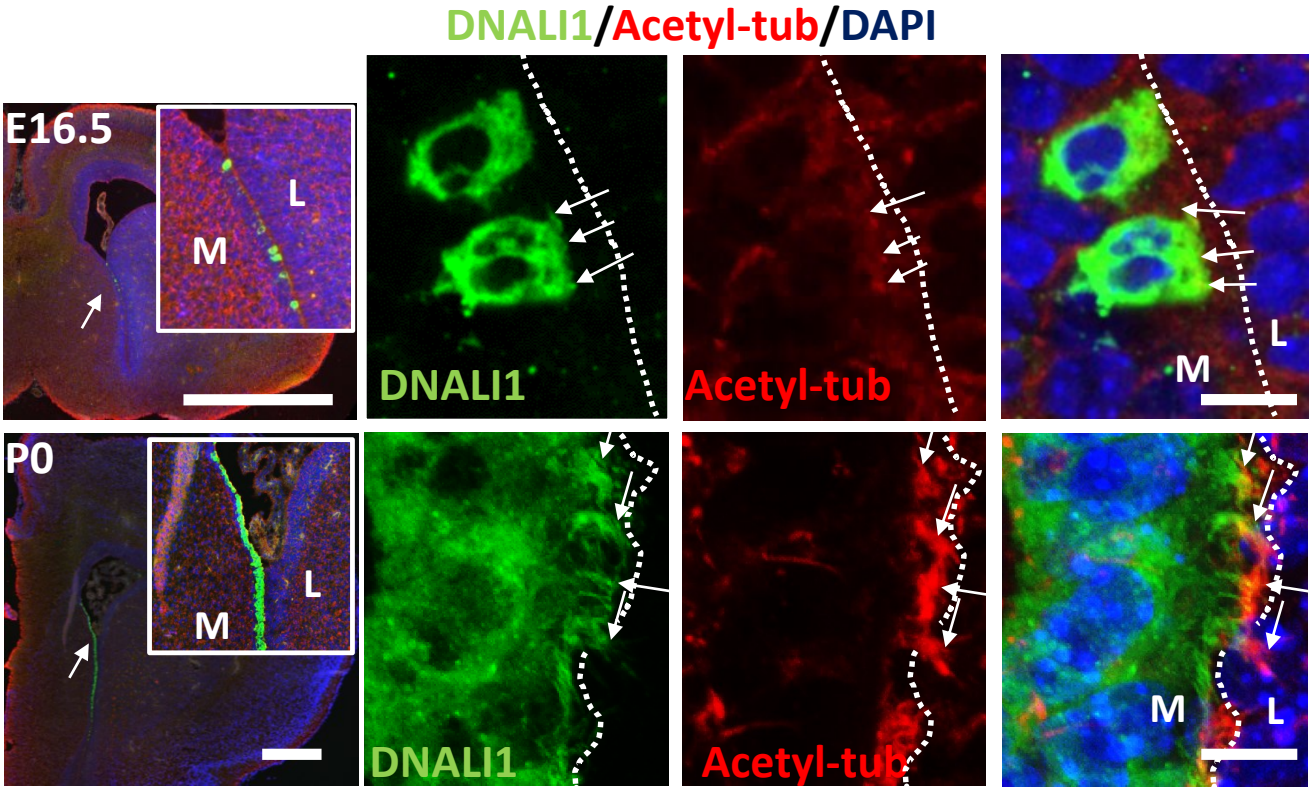

Supplemental Figure 4. Expression of DNALI1 and acetylated tubulin in the developing ependymal cells.
At E16, cytoplasmic expression of DNALI1 was found in fractions of ependymal cells on the medial side of the forebrain ventricles (top). Acetylated tubulin-positive cilia (white arrows) are just about to extend from their apical surface. At P0, most of the ependymal cells express DNALI1 in both cytoplasm and acetylated tubulin-positive cilia (white arrows) (bottom). Scale bars 1mm (left), and 10 µm (right)

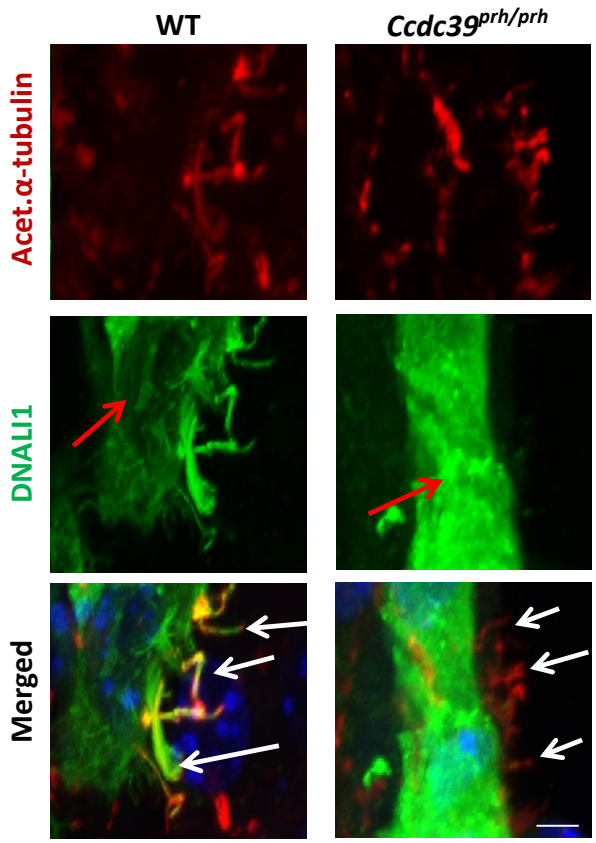

Supplemental Figure 5. *Ccdc39* regulates DNALI1 expression and is essential for targeting the inner dynein arm protein to ependymal cilia.
Immunofluorescent confocal images of ependymal cells stained with DNALI1 (green) and acetylated α-tubulin (red) antibodies in P9 wild-type and *Ccdc39*$^{prh/prh}$ forebrain. DNALI1 was not detected in the axoneme of the *Ccdc39*$^{prh/prh}$ mutant ependymal cilia (white arrow). Note the abnormal cytoplasmic accumulation of DNALI1 in the *Ccdc39*$^{prh/prh}$ mutant cells. (Scale bar 10 µm).

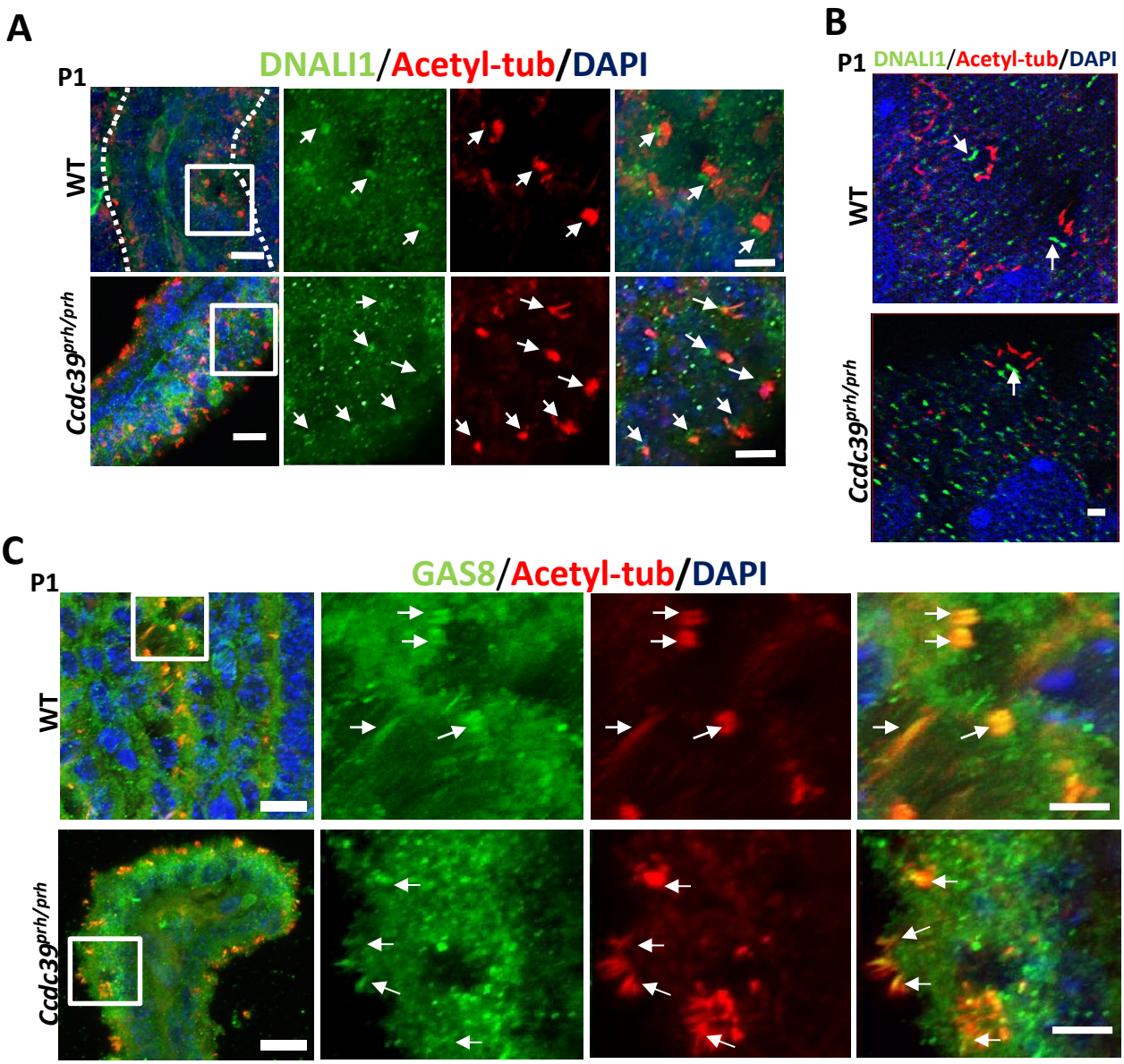

Supplemental Figure 6. Expression patterns of motile cilia markers DNALI1 and GAS8 are maintained in the *Ccdc39*$^{prh/prh}$ mutant.

(A) Immunofluorescent confocal images of choroid plexus cells in the P1 mouse brain stained with DNALI1 (green) and acetylated tubulin (red) antibodies.

(B) SRRF images of the choroid plexus cilia stained with DNALI1 (green) and acetylated tubulin (red) in P1 wild-type and *Ccdc39*$^{prh/prh}$ brains. Note that DNALI1 localizes at the base of cilia in both wild-type and the mutant choroid plexus cilia (white arrows).

(C) Immunofluorescent confocal images of choroid plexus cells in the P1 mouse brain stained with GAS8 (green) and acetylated tubulin (red) antibodies. GAS8 localizes within the axoneme of both wild-type and the mutant choroid plexus cilia (white arrows).

Scale bars, 10 μm (A and C, left), 5 μm (A and C, right), and 1 μm (B).

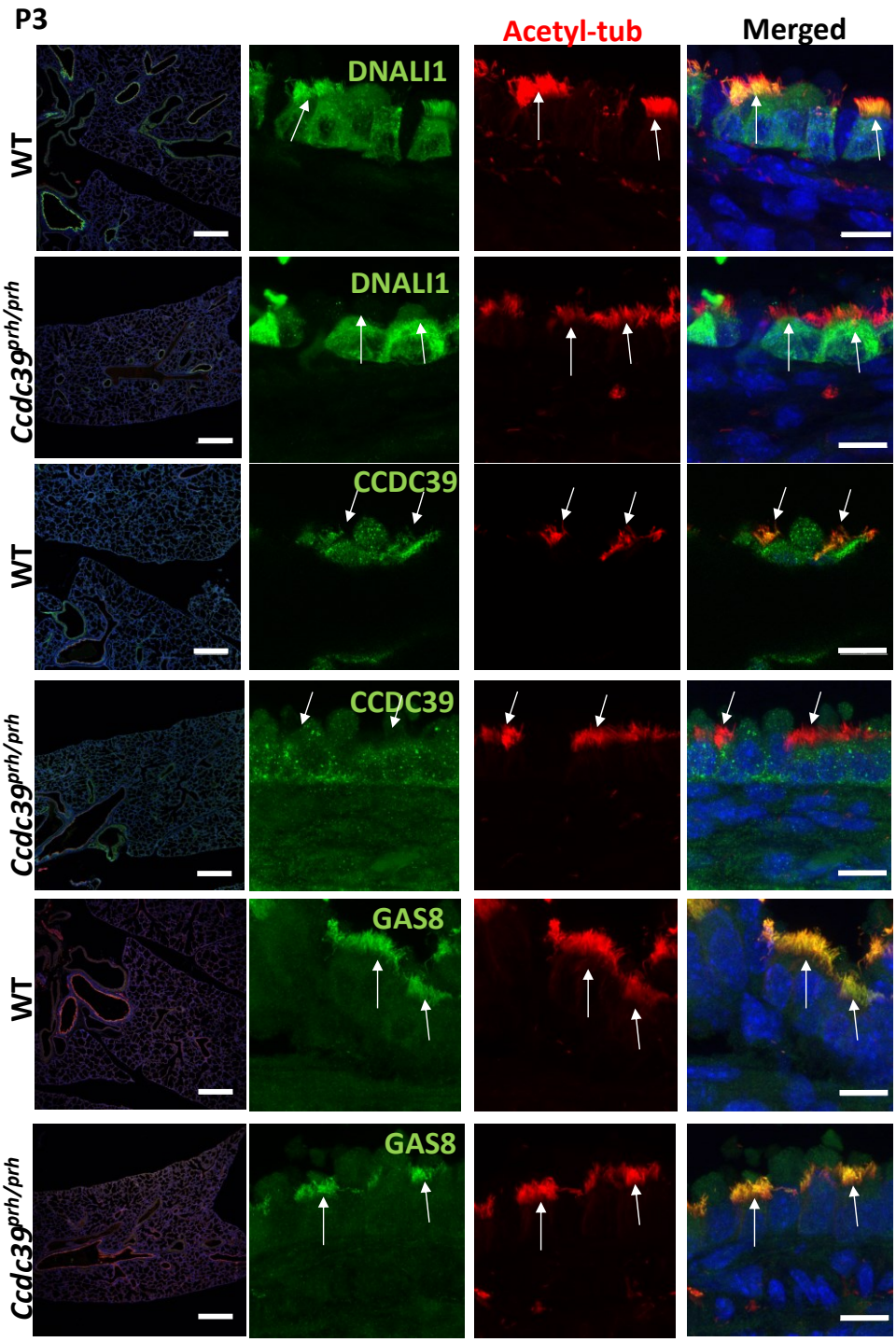

Supplemental Figure 7. *Ccdc39* is localized within the axoneme and is essential for targeting DNALI1 in the airway cilia.
Immunofluorescent confocal images of ependymal cells stained with DNALI1, CCDC39, or GAS8 (green) with acetylated α-tubulin (red) antibodies in P3 wild-type and *Ccdc39*$^{prh/prh}$ the lung. DNALI1 was not detected in the axoneme of the *Ccdc39*$^{prh/prh}$ mutant bronchial cilia (white arrow). Note the mutation did not affect GAS8 (Scale bars; left 500 µm, right 10 µm).

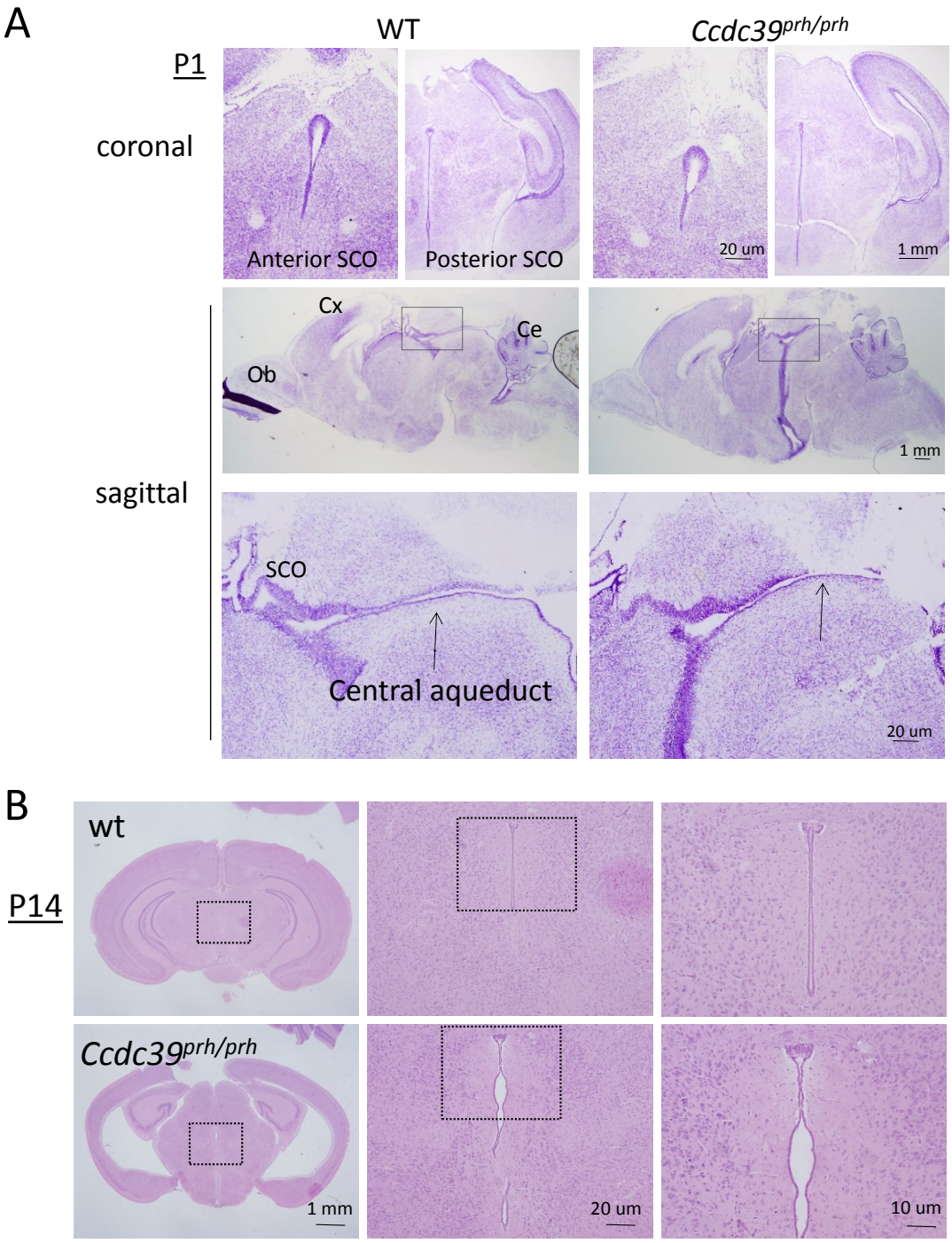

Supplemental Figure 8. Physical obstruction of the central aqueduct was not found in early postnatal *Ccdc39*$^{prh/prh}$ mutants.

(A) Representative images of serial brain sections of P1 wild-type and *Ccdc39*$^{prh/prh}$ mutant mice in the Nissl staining. Note that there is normal opening of the central aqueduct (arrow) and SCO in the mutant at P1 when they have ventriculomegaly phenotype.

(B) Hematoxylin and eosin staining of P14 wild-type and *Ccdc39*$^{prh/prh}$ mutant brain sections. The mutant mice developed abnormally lined ependymal cell layers that led to a wider opening in the rostral part of the central aqueduct.